ResearchGate

See discussions, stats, and author profiles for this publication at: https://www.researchgate.net/publication/6330673

Phenalenyl-Based Neutral Radical Molecular Conductors: Substituent Effects on Solid-State Structures and Properties

ARTICLE *in* JOURNAL OF THE AMERICAN CHEMICAL SOCIETY · JULY 2007

Impact Factor: 12.11 · DOI: 10.1021/ja070103i · Source: PubMed

CITATIONS
26

READS
41

7 AUTHORS, INCLUDING:

M.E. Itkis
University of California, Riverside
174 PUBLICATIONS **12,112** CITATIONS
SEE PROFILE

Bruno Donnadieu
University of California, Riverside
221 PUBLICATIONS **7,300** CITATIONS
SEE PROFILE

Available from: M.E. Itkis
Retrieved on: 26 January 2016

J|A|C|S
ARTICLES
Published on Web 05/15/2007

Phenalenyl-Based Neutral Radical Molecular Conductors: Substituent Effects on Solid-State Structures and Properties

Sushanta K. Pal,[†] Mikhail E. Itkis,[†] Fook S. Tham,[†] Robert W. Reed,[‡] Richard T. Oakley,[‡] Bruno Donnadieu,[†] and Robert C. Haddon*,[†]

Contribution from the Departments of Chemistry and Chemical & Environmental Engineering, University of California, Riverside, California 92521-0403, and Department of Chemistry, University of Waterloo, Waterloo, Ontario N2L 3G1, Canada

Received January 5, 2007; E-mail: haddon@ucr.edu

Abstract: We report the preparation, crystallization, and solid-state characterization of cycloheptyl and cyclooctyl-substituted spirobiphenalenyl radicals and the corresponding σ-dimer of the cyclooctyl derivative. The crystal structure shows that the cycloheptyl radical (**9**) is monomeric in the solid state, with the molecules packed in an unusual one-dimensional (1-D) fashion that we refer to as a π-chain structure, whereas the cyclooctyl variant exists both as π-dimer **10** and σ-dimer **10d**. The neutral radical **9** shows the temperature-independent Pauli paramagnetism characteristic of a metal with a magnetic susceptibility, $\chi_p \approx 4.5 \times 10^{-4}$ emu/mol and is assigned a resonating valence bond (RVB) ground state. We highlight the relationship between the magnetic properties of the Heisenberg antiferromagnet and the RVB ground state in 1-D and further elucidate the electronic structure of this new class of compounds. Magnetic susceptibility measurements show that **10** is a diamagnetic π-dimer, whereas **10d** is a diamagnetic σ-dimer. Extended Hückel calculations for **9** indicate that the solid is a one-dimensional organic metal with a bandwidth of about 0.4 eV. Pressed pellet conductivity measurements indicate values of $\sigma_{RT} = 1.5 \times 10^{-3}$ S/cm for compound **9** and $\sigma_{RT} = 1.0 \times 10^{-6}$ S/cm for compound **10**. The structural results and transport properties are discussed in the light of extended Hückel theory band structure calculations and DFT investigations of the electronic structure of related compounds.

Introduction

In the last 30 years a number of organic conductors and superconductors have been synthesized based on tetrathiafulvalene (TTF) derivatives[1,2] and C_{60}.[3−5] These highly conducting compounds are charge-transfer salts, where the charge carriers are generated by the formation of radical ions. Recent work has led to the development of single-component organometallic neutral molecular conductors with extended tetrathiafulvalene (TTF) dithiolate ligands, such as $[Ni(tmdt)_2]$ (tmdt = trimethylenetetrathiafulvalenedithiolate), which exhibit metallic conductivity and three-dimensional (3-D) Fermi surfaces for both holes and electrons.[6−8] These conductors can be classified as single-component molecular conductors based on internal charge transfer.

Molecular conductors based on single-component neutral radicals represent an alternative approach to the design of lattices with spins; an array of radicals in a neutral lattice could function like atoms in an elemental metal.[9,10] The phenalenyl molecule is a good candidate for designing molecular conductors because of its high symmetry (D_{3h}) and its ability to form three stable redox species: cation, radical, and anion.[11−13] Certain paramagnetic phenalenyl radicals undergo facile dimerization either by π-association or by σ-association, and recent progress in phenalenyl chemistry has led to the isolation of the substituted forms of the radical in the crystalline state.[14−21] In fact, the intermolecular π-association of 2,5,8-tri-*tert*-butylphenalenyl

[†] Departments of Chemistry and Chemical & Environmental Engineering, University of California.
[‡] Department of Chemistry, University of Waterloo.

(1) Williams, J. M.; Ferraro, J. R.; Thorn, R. J.; Carlson, K. D.; Geiser, U.; Wang, H. H.; Kini, A. M.; Whangbo, M.-H. *Organic Superconductors* (*Including Fullerenes*); Prentice Hall: Englewood Cliffs, 1992.
(2) Ishiguro, T.; Yamaji, K.; Saito, G. *Organic Superconductors*, 2nd ed.; Springer-Verlag: Berlin, 1998; Vol. 88.
(3) Haddon, R. C.; et al. *Nature* **1991**, *350*, 320−322.
(4) Hebard, A. F.; Rosseinsky, M. J.; Haddon, R. C.; Murphy, D. W.; Glarum, S. H.; Palstra, T. T. M.; Ramirez, A. P.; Kortan, A. R. *Nature* **1991**, *350*, 600.
(5) Haddon, R. C. *Acc. Chem. Res.* **1992**, *25*, 127.
(6) Tanaka, H.; Okano, Y.; Kobayashi, H.; Suzuki, W.; Kobayashi, A. *Science* **2001**, *291*, 285−287.
(7) Tanaka, H.; Tokumoto, M.; Ishibashi, S.; Graf, D.; Choi, E. S.; Brooks, J. S.; Yasuzuka, S.; Okano, Y.; Kobayashi, H.; Kobayashi, A. *J. Am. Chem. Soc.* **2004**, *126*, 10518−10519.
(8) Kobayashi, A.; Sasa, M.; Suzuki, W.; Fujiwara, E.; Tanaka, H.; Tokumoto, M.; Okano, Y.; Fujiwara, H.; Kobayashi, H. *J. Am. Chem. Soc.* **2004**, *126*, 426−427.
(9) Haddon, R. C. *Nature* **1975**, *256*, 394−396.
(10) Haddon, R. C. *Aust. J. Chem* **1975**, *28*, 2343−2351.
(11) Reid, D. H. *Q. Rev.* **1965**, *19*, 274−302.
(12) Reid, D. H. *Chem. Ind.* **1956**, 1504−1505.
(13) Reid, D. H. *Tetrahedron* **1958**, *3*, 339−352.
(14) Goto, K.; Kubo, T.; Yamamoto, K.; Nakasuji, K.; Sato, K.; Shiomi, D.; Takui, T.; Kubota, M.; Kobayashi, T.; Yakusi, K.; Ouyang, J. *J. Am. Chem. Soc.* **1999**, *121*, 1619−1620.
(15) Fukui, K.; Sato, K.; Shiomi, D.; Takui, T.; Itoh, K.; Gotoh, K.; Kubo, T.; Yamamoto, K.; Nakasuji, K.; Naito, A. *Synth. Met.* **1999**, *103*, 2257−2258.
(16) Koutentis, P. A.; Chen, Y.; Cao, Y.; Best, T. P.; Itkis, M. E.; Beer, L.; Oakley, R. T.; Brock, C. P.; Haddon, R. C. *J. Am. Chem. Soc.* **2001**, *123*, 3864−3871.
(17) Takano, Y.; Taniguchi, T.; Isobe, H.; Kubo, T.; Morita, Y.; Yamamoto, K.; Nakasuji, K.; Takui, T.; Yamaguchi, K. *J. Am. Chem. Soc.* **2002**, *124*, 11122−11130.

Scheme 1

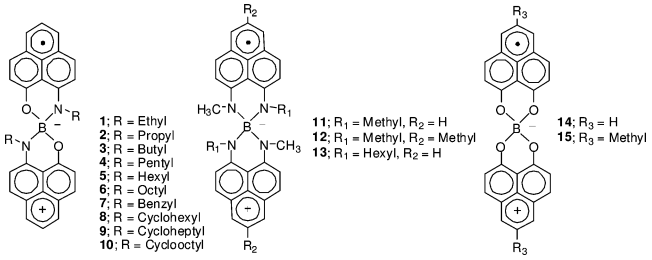

Scheme 2

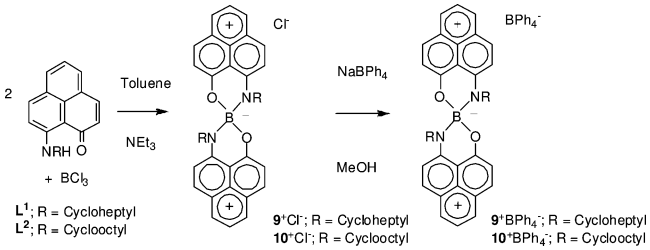

radicals can take place either by formation of a two-electron bond to form a π-dimer (radical−radical pair) or by formation of a one-electron bond to form a π-pimer (radical−cation pair).[20]

For some time we have attempted to prepare an intrinsic molecular metal, that is a solid composed of a single molecular species that would function as a classical (mono) atomic metal and superconductor.[22,23] In our pursuit of phenalenyl-based neutral radical molecular conductors, we have reported a series of spiro-bis(1,9-disubstituted phenalenyl) boron neutral radicals **1**−**15** (Scheme 1).[24−32] Following the discovery of the first boron containing neutral radical molecular conductor (**5**) bearing the phenalenyl-based N,O ligand system,[24] we identified a class of dimeric neutral radical molecular conductors (**1** and **3**) differing only in the length of the alkyl groups (Scheme 1). Radicals **1** and **3** form face-to-face π-dimers so that there is selective registry between spin-bearing carbon atoms of the phenalenyl units.[25] These dimeric neutral radicals (**1** and **3**) simultaneously exhibit bistability in three physical channels: magnetic, electrical, and optical,[33] which has been rarely realized in a single system.[34] Interestingly, these crystals undergo phase transitions from high-temperature paramagnetic states to low-temperature diamagnetic states, accompanied by an increase in the conductivities by 2 orders of magnitude. A distinctive feature of these molecular solids is the absence of any obvious conducting pathway(s). These radicals do not stack in the solid state, and the intermolecular carbon···carbon contacts are all larger than the sum of the van der Waals distances. Recently, we reported the first one-dimensional (1-D) phenalenyl-based neutral radical molecular conductor **7**.[28] In the solid state, the phenalenyl units of **7** pack orthogonally in the *x*- and *z*-directions, whereas the phenalenyl units are parallel to each other in the *y*-direction in a π-step structure.

We reported the first example of light-mediated C−C σ-bond formation between two radical molecules,[29] and **6** exists as two different forms: a free radical semiconductor and an insulating σ-dimer, and the formation of these crystalline forms is dictated by the presence or absence of light. Most recently, we reported the resonating valence bond (RVB) ground state in the quasi-1-D phenalenyl-based neutral radical conductor **8**,[31] and oxygen-functionalized phenalenyl-based neutral radical molecular conductors (**14**−**15**).[32] Crystals of **8** show the highest room-temperature conductivity of $\sigma_{RT} = 0.3$ S/cm among the phenalenyl-based neutral radical conductors and a high-symmetry crystal structure; the compound displays the temperature-independent Pauli paramagnetism characteristic of a metal. Recent ab initio band structure calculations on this material have been interpreted in terms of a 1-D organic metal.[35,36]

We have now crystallized two new members of the family of spiro-bis(1,9-disubstituted phenalenyl) boron compounds (**9** and **10**), one of which may be induced to crystallize as a σ-dimer (**10d**); the new molecules differ only in the alkyl substituent from previous members in the series (**1**−**8**) but adopt distinct solid-state structures. There are numbers of difficulties that must be surmounted if molecular metals and superconductors based on phenalenyl are to be realized, and the current class of compounds directly addresses some of these problems. The presence of perpendicular π-systems usually inhibits the simple 1-D stacking that is characteristic of many organic charge-transfer salts. Radical **7** adopts a 1-D π-step structure, but the packing constraints do not allow efficient overlap, and this compound circumvents the usual charge density wave instabilities that are characteristic of 1-D systems by adopting the RVB ground state.

In the present paper, we report the synthesis, crystallization, and solid-state properties of radical **9**, π-dimer **10**, and σ-dimer **10d**. We assess the strength of the interaction between the molecules in the lattice by using extended Hückel theory (EHT). In the solid state, cycloheptyl radical **9** does not form a simple σ- or π-dimer, nor does it remain strictly monomeric; in this respect it bears a strong resemblance to the structure of **8**.[31] The unit cell of cycloheptyl radical contains two molecules, the asymmetric unit is half of the molecule, and the molecule is

(18) Morita, Y.; Aoki, T.; Fukui, K.; Nakazawa, S.; Tamaki, K.; Suzuki, S.; Fuyuhiro, A.; Yamamoto, K.; Sato, K.; Shiomi, D.; Naito, A.; Takui, T.; Nakasuji, K. *Angew. Chem., Int. Ed.* **2002**, *41*, 1793−1796.
(19) Takano, Y.; Taniguchi, T.; Isobe, H.; Kubo, T.; Morita, Y.; Yamamoto, K.; Nakasuji, K.; Takui, T.; Yamaguchi, K. *Chem. Phys. Lett.* **2002**, *358*, 17−23.
(20) Small, D.; Zaitsev, V.; Jung, Y.; Rosokha, S. V.; Head-Gordon, M.; Kochi, J. K. *J. Am. Chem. Soc.* **2004**, *126*, 13850−13858.
(21) Beer, L.; Mandal, S. K.; Reed, R. W.; Oakley, R. T.; Tham, F. S.; Donnadieu, B.; Haddon, R. C. *Cryst. Growth Des.* **2007**, *7*, 101−108.
(22) Haddon, R. C.; Wudl, F.; Kaplan, M. L.; Marshall, J. H.; Cais, R. E.; Bramwell, F. B. *J. Am. Chem. Soc* **1978**, *100*, 7629−7633.
(23) Haddon, R. C.; Chichester, S. V.; Stein, S. M.; Marshall, J. H.; Mujsce, A. M. *J. Org. Chem.* **1987**, *52*, 711−712.
(24) Chi, X.; Itkis, M. E.; Patrick, B. O.; Barclay, T. M.; Reed, R. W.; Oakley, R. T.; Cordes, A. W.; Haddon, R. C. *J. Am. Chem. Soc.* **1999**, *121*, 10395−10402.
(25) Chi, X.; Itkis, M. E.; Kirschbaum, K.; Pinkerton, A. A.; Oakley, R. T.; Cordes, A. W.; Haddon, R. C. *J. Am. Chem. Soc.* **2001**, *123*, 4041−4048.
(26) Chi, X.; Itkis, M. E.; Reed, R. W.; Oakley, R. T.; Cordes, A. W.; Haddon, R. C. *J. Phys. Chem. B* **2002**, *106*, 8278−8287.
(27) Chi, X.; Itkis, M. E.; Tham, F. S.; Oakley, R. T.; Cordes, A. W.; Haddon, R. C. *Int. J. Quant. Chem.* **2003**, *95*, 853−865.
(28) Pal, S. K.; Itkis, M. E.; Reed, R. W.; Oakley, R. T.; Cordes, A. W.; Tham, F. S.; Siegrist, T.; Haddon, R. C. *J. Am. Chem. Soc.* **2004**, *126*, 1478−1484.
(29) Liao, P.; Itkis, M. E.; Oakley, R. T.; Tham, F. S.; Haddon, R. C. *J. Am. Chem. Soc.* **2004**, *126*, 14297−14302.
(30) Mandal, S. K.; Itkis, M. E.; Chi, X.; Samanta, S.; Lidsky, D.; Reed, R. W.; Oakley, R. T.; Tham, F. S.; Haddon, R. C. *J. Am. Chem. Soc.* **2005**, *127*, 8185−8196.
(31) Pal, S. K.; Itkis, M. E.; Tham, F. S.; Reed, R. W.; Oakley, R. T.; Haddon, R. C. *Science* **2005**, *309*, 281−284.
(32) Mandal, S. K.; Samanta, S.; Itkis, M. E.; Jensen, D. W.; Reed, R. W.; Oakley, R. T.; Tham, F. S.; Donnadieu, B.; Haddon, R. C. *J. Am. Chem. Soc.* **2006**, *128*, 1982−1994.
(33) Itkis, M. E.; Chi, X.; Cordes, A. W.; Haddon, R. C. *Science* **2002**, *296*, 1443−1445.
(34) Miller, J. S. *Angew. Chem., Int. Ed.* **2003**, *42*, 27−29.
(35) Huang, J.; Kertesz, M. *J. Am. Chem. Soc.* **2006**, *128*, 1418−1419.
(36) Bohlin, J.; Hansson, A.; Stafstrom, S. *Phys. Rev. B* **2006**, *74*, 155111.

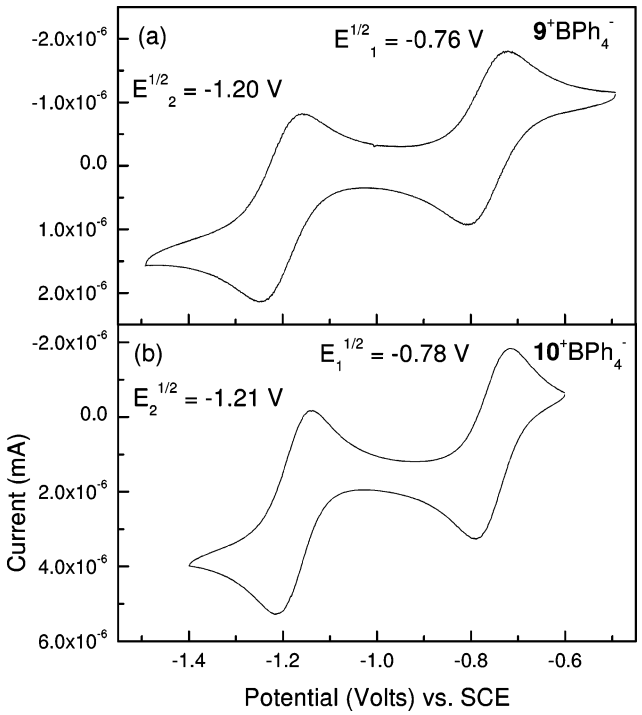

Figure 1. Cyclic voltammetry of (a) $\mathbf{9}^+BPh_4^-$, (b) $\mathbf{10}^+BPh_4^-$ in acetonitrile, reference to SCE via internal ferrocene (not shown).

located on a two-fold rotation axis parallel to the *y*-axis. In **9**, the phenalenyl units in the *xz*-plane pack parallel to each other, the π-overlap occurs between the spin-bearing carbon of the phenalenyl unit, and this π-overlap is continuous throughout the lattice which we refer to as a 1-D π-chain structure. As shown by the band structure calculations, this provides a very effective conducting pathway in crystals of cycloheptyl radical **9** where each of the active carbon atoms is involved in overlap with its nearest neighbor. On changing the substituents on the nitrogen atom from cycloheptyl to cyclooctyl, the compound is found to crystallize as either a diamagnetic π-dimer **10** or a diamagnetic σ-dimer **10d**, depending on the choice of reducing agent.

Results and Discussion

Preparation, Solution Properties, and Crystallization of 9, 10 (Radical), and 10d (σ-Dimer). The synthesis of radical **9** and **10** followed the same basic procedure that was used to prepare radicals **1**−**8**.[24,25] We prepared the cycloheptyl and cyclooctyl variant via the chloride salts ($\mathbf{9}^+Cl^-$ and $\mathbf{10}^+Cl^-$) but finally employed the tetraphenylborate salts ($\mathbf{9}^+BPh_4^-$ and $\mathbf{10}^+BPh_4^-$) to obtain the required solubility properties and in order to purify the salts (Scheme 2). Triethylamine was added to the reaction mixture in order to prevent the formation of the ligand hydrochloride salt; this led to contamination of the product by triethylamine hydrochloride which was removed on recrystallization of the tetraphenylborate salt. Compound $\mathbf{9}^+BPh_4^-$ and $\mathbf{10}^+BPh_4^-$ precipitated as air-stable but light-sensitive orange solids that could be purified by recrystallization from methanol/acetonitrile and dichloromethane to give material suitable for radical preparation and crystal growth.

The electrochemistry of $\mathbf{9}^+BPh_4^-$ and $\mathbf{10}^+BPh_4^-$ are shown in Figure 1; the compounds show a well-behaved double reduction. The first reduction potential was characterized as the

Scheme 3

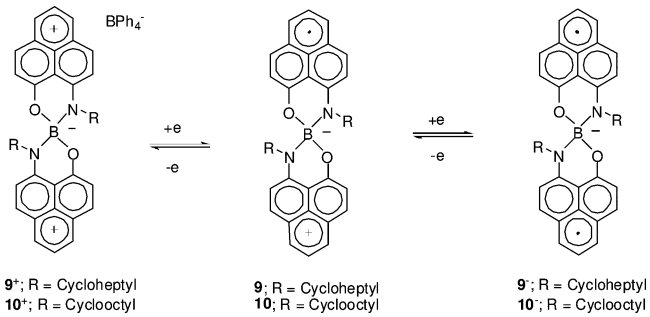

reduction of the cation to radical, and the second reduction potential corresponds to radical-to-anion reduction (Scheme 3). The disproportionation potentials $\Delta E_{2-1} = (E_2^{1/2} - E_1^{1/2})$ of $\mathbf{9}^+$ and $\mathbf{10}^+$ are −0.44 V and −0.43 V and are higher than the values found for the alkyl-, benzyl-, and cyclohexyl-substituted compounds (**1**−**8**, $\Delta E_{2-1} \approx -0.34$ V). The ΔE_{2-1} value largely determines the on-site Columbic correlation energy (*U*) in the solid state and is well established as an important discriminator for organic metals.[37,38]

We crystallized **9** and **10** by using a chemical reductant in an H-cell and obtained a moderate yield of high-quality, black needles of the radicals. Cobaltocene [bis(cyclopentadienyl)Co-(II), Cp_2Co] was used as reducing agent because its oxidation potential falls between the $E_1^{1/2}$ and $E_2^{1/2}$ reduction potentials of $\mathbf{9}^+BPh_4^-$ and $\mathbf{10}^+BPh_4^-$.[24,25] To ensure high crystal quality the H-cell was loaded in a drybox, and the solvent (acetonitrile) was degassed a minimum of three times on a vacuum line before mixing reductant and salt. Crystal growth was apparent after overnight standing, and the crystals reached their optimum size and quality in about 5−7 days. Although solutions of the radical are extremely oxygen sensitive, the crystals are sufficiently stable to allow ambient chemical analyses, X-ray crystal structure determination, and solid-state measurements.

We had previously found that the crystal quality of **8** could be improved by replacing cobaltocene with bis(pentamethyl-cyclopentadienyl)nickel(II) (Cp^*_2Ni), for the reduction of the salt.[31] Because the oxidation potential of Cp^*_2Ni ($E_1^{1/2} = -0.65$,[39] −0.69 V[40]) is lower than that of Cp_2Co ($E_1^{1/2} = -0.91$,[39] −0.94 V[41]) and slightly lower than the first reduction potential of the salts, radical crystallization with Cp^*_2Ni occurs more slowly than with Cp_2Co. Typically, nucleation of the radical crystals requires overnight standing when Cp^*_2Ni is used as a reducing agent, but in the case of Cp_2Co the crystals appear in a few hours. Surprisingly, when we employed Cp^*_2Ni as the reducing agent for $\mathbf{10}^+BPh_4^-$, long, black needles of **10d** crystallized from acetonitrile. The crystalline forms cannot be distinguished by eye, but can be identified by near-IR transmittance spectroscopy of single crystals. In the beginning, we expected the simultaneous formation of both crystalline phases, but after careful investigation of the occurrence domain of the crystallization, we were able to identify the reducing agent as the critical parameter (Scheme 4). When we use cobaltocene

(37) Garito, A. F.; Heeger, A. J. *Acc. Chem. Res.* **1974**, *7*, 232−240.
(38) Torrance, J. B. *Acc. Chem. Res.* **1979**, *12*, 79−86.
(39) Robbins, J. L.; Edelstein, N.; Spencer, B.; Smart, J. C. *J. Am. Chem. Soc.* **1982**, *104*, 1882−1893.
(40) Ryan, M. F.; Richardson, D. E.; Lichtenberger, D. L.; Gruhn, N. E. *Organometallics* **1994**, *13*, 1190−1199.
(41) Holloway, J. D. L.; Geiger, J. W. E. *J. Am. Chem. Soc.* **1979**, *101*, 2038−2044.

Scheme 4

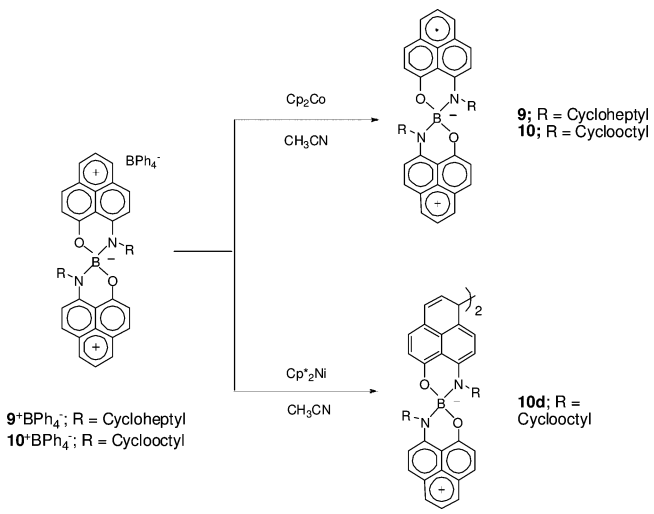

as reducing agent, the π-dimer **10** is formed exclusively, whereas the use of Cp^*_2Ni leads to the σ-dimer **10d** as the only product. The use of Cp^*_2Ni as reducing agent for $\mathbf{8}^+BPh_4^-$ leads solely to the formation of radical **8**.[31] We have previously observed light-mediated σ-dimerization in octyl radical **6**, but we cannot explain why this behavior does not occur with other members of the series (**1**−**5**, **7**−**9**).[29]

X-ray Crystal Structures of 9, 10 and 10d. The X-ray crystal structures of **9**, **10** (π-dimer), and **10d** (σ-dimer) were determined at $T = 100$ K (Figure 2), and the crystal data are summarized in Table 1. The distinctive features of the phenalenyl packing are a π-chain with a separation between phenalenyl rings of 3.26 Å (radical, **9**) (Figure 3), a π-dimer with a separation between phenalenyl rings of 3.16 Å (**10**) (Figure 4) and a σ-dimer with a long C–C single bond (1.612 Å) between the symmetry-related C16 atoms (**10d**, Figures 2c and 5).

Compound **9** gave rise to monoclinic, black crystals of space group $P2/n$ with two molecules in the unit cell. The most important point for our purposes is the absence of simple σ- or π-dimerization, even though we did not employ bulky substituents at the active position of the phenalenyl nucleus in order to suppress intermolecular carbon···carbon bond formation.[22,23] Table 1 provides crystal data, and Figure 2a shows an ORTEP drawing of the molecule together with the atom numbering. The unit cell of crystalline **9** is shown in Figure 3a. The molecule is spiro-conjugated, and the dihedral angle between the two halves of the molecule is 86.4°. The asymmetric unit is half of the molecule, and the phenalenyl group is almost planar. The molecule is located on a two-fold rotation axis parallel to the *y*-axis. There are many short C···C contacts between neighboring molecules in the *xz*-plane and also along the *y*-direction. In the *x*- and *z*-directions the phenalenyl rings are parallel to one another (Figure 3a). The closest carbon···carbon distances along the π-chain vary from 3.27 to 3.36 Å (Figure 3d), and thus all interradical distances are shorter than the van der Waals separation. The π-chain overlap occurs along the diagonal of the *xz*-plane, and the π overlap occurs only between the spin-bearing carbon atoms of the phenalenyl ring. The molecules are almost superimposed at the spin-bearing carbon positions, so the overlap between molecules is very effective (see band structure discussion below). The average interplanar separation between the two molecules is 3.26 Å ($T = 100$ K), which is

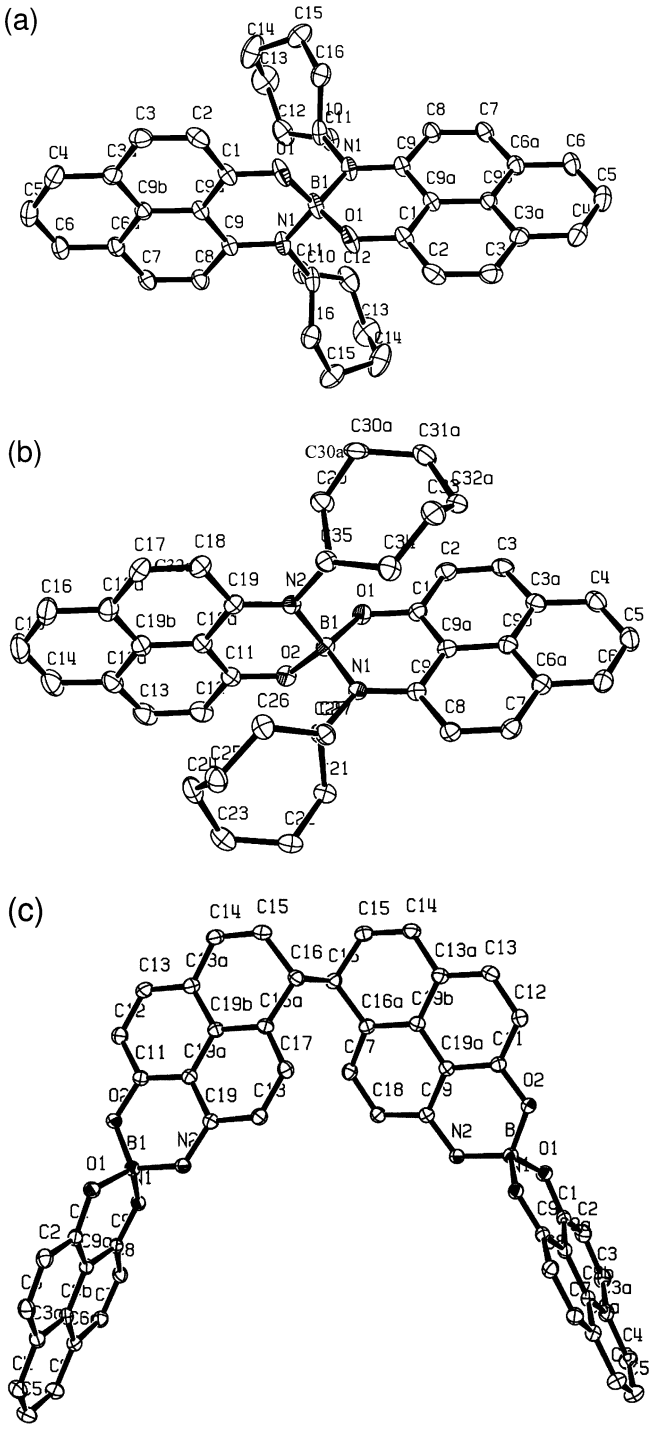

Figure 2. ORTEP drawing of the solid-state structure of (a) cycloheptyl radical (**9**), (b) cyclooctyl radical (**10**), and (c) cyclooctyl σ-dimer (**10d**), with the cyclooctyl groups omitted.

less than the van der Waals distances between two carbon atoms (3.4 Å). These interatomic distances may be compared with the mean plane separations seen in the ethyl radical (**1**): 3.18 Å at $T = 100$ K, diamagnetic) and 3.31 Å ($T = 173$ K, paramagnetic),[25] Pauli paramagnetic radical **8**: 3.28 Å (223 K),[31] Pauli paramagnetic radical **14**: 3.17 Å (100 K), 3.22 Å (293 K), and Pauli paramagnetic radical **15**: 3.26 Å, 3.29 Å (100 K), 3.30 Å, 3.30 Å (300 K).[32]

The packing in the *y*-direction is quite different from the packing in the *x*- and *z*-directions. The molecules form a stack along the *y*-axis (Figure 3b). The phenalenyl rings have a weak

Table 1. Crystal Data for **9**−**10d**

	9	**10**	**10d**
formula	$C_{40}H_{40}N_2O_2B$	$C_{44}H_{47}BN_3O_2$	$C_{84}H_{88}B_2N_4O_4$
F_w	591.55	660.66	1239.20
temp	100(2) K	100(2) K	100(2) K
crystal system	monoclinic	triclinic	monoclinic
space group	$P2/n$	$P\bar{1}$	$C2/c$
a, Å	9.5948(4)	11.6514(16)	17.7417(6)
b, Å	9.3265(4)	13.2224(18)	14.1192(5)
c, Å	16.4410(7)	13.568(3)	25.9092(9)
α, deg	90	106.025(4)	90
β, deg	92.8950(10)	105.873(4)	99.1190(10)
γ, deg	90	110.198(3)	90
V, Å^3	1469.36(11)	1720.7(5)	6408.2(4)
Z	2	2	4
crystal size, mm	0.63 × 0.24 × 0.07	0.26 × 0.11 × 0.05	0.25 × 0.12 × 0.10
goodness of fit on F^2	1.031	1.022	1.022
final R indices [$I > 2\sigma(I)$]	R1 = 0.0477, wR2 = 0.1362	R1 = 0.0474, wR2 = 0.1140	R1 = 0.0497 wR2 = 0.1264
R indices (all data)	R1 = 0.0621 wR2 = 0.1480	R1 = 0.0780 wR2 = 0.1287	R1 = 0.0740 wR2 = 0.1413

interaction (3.83 Å) between the spin-bearing carbons of the nearest neighbors, and we termed these interactions a π-step pattern (Figure 3c). The closest carbon···carbon distances between molecules along the y-direction are 3.83 Å for spin-bearing carbon atoms (Figure 3c). The molecules are almost superimposed at these positions, but as the distances between the spin-bearing carbon is quite long, there is little dispersion in the band structure along this direction.

A similar packing pattern was observed in the case of cyclohexyl radical (**8**). The only differences between these two structures are the carbon···carbon distances between phenalenyl rings. In **8** and **9** the mean plane separations along the π-chains are similar: 3.28 Å in case of **8** and 3.26 Å for **9**. However, there are significant differences in the carbon···carbon distances along the y-axis between these two structures: the closest distance is 3.38 Å (for **8**), whereas the same distance for **9** is 3.83 Å (greater than the van der Waals distances between a pair of carbon atoms).

The X-ray crystal structure of radical **10** was determined at $T = 100$ K, and the crystal data are summarized in Table 1. Figure 2b shows the ORTEP drawing of the molecule together with atom numbering. A molecule of acetonitrile is present in the crystal, but the crystals are quite stable even under vacuum. The unit cell of **10** is shown in Figure 4a. The black crystals of **10** gave a triclinic unit cell (space group $P\bar{1}$, $Z = 2$), and the molecules exists as π-dimers with a separation between the molecular planes of 3.16 Å; on the basis of the magnetic data, we refer to **10** as a diamagnetic π-dimer; the phenalenyl planes are parallel to each other, and π overlap occurs between the spin-bearing carbon atoms of the phenalenyl units.

The carbon ···carbon distance between phenalenyl units varies from 3.13 Å to 3.25 Å (Figure 4b) and all interradical distances are much shorter than the van der Waals separations for carbon atoms.

The black crystals of **10d** gave a monoclinic unit cell (space group $C2/c$, $Z = 4$, Figure 5a); the C−C single bond between the symmetry-related C16 atoms is significantly longer (1.612 Å) than the normal sp^3 C−C single bond length (1.54 Å), but comparable to the analogous σ-bond in **6** (1.599 Å).[29] While this bond is relatively unstrained, its length is comparable to those of strained C−C bonds and to those of carbon σ-bonds that form at the expense of a delocalized π-system. The length of the central C−C bond in Gomberg-type dimers such as hexaphenylethane and its derivatives is generally greater than 1.6 Å,[42−44] although shorter than the bond lengths that occur in charged π-dimers.[45−50]

We also determined the structure at room temperature, but there are no significant differences in packing or in the carbon···carbon distances. The packing of the σ-dimer is quite interesting, and the asymmetric unit is half of the molecule; it also forms a π-chain throughout the crystal lattice. The π-overlap occurs between the non-σ-bonded half of the molecule, and the overlap occurs with registry between the spin-bearing carbon atoms although the molecules are diamagnetic; the carbon···carbon distances vary from 3.39 to 3.48 Å (Figure 5b) which is close to the van der Waals separation.

The length of the σ-bond in **10d** is comparable to that of the intercage C−C bond (1.597 Å) of the $(C_{60}^-)_2$ dimer;[51,52] the reversible formation of this dimer occurs at around 220 K, and this raises the question as to whether the crystalline forms of **10d** might be interconvertible; however, magnetic susceptibility measurements of **10d** show a diamagnetic state from 4 to 344 K (Figure 6).

Magnetic Susceptibility and Conductivity of 9, 10, and 10d. We measured the magnetic susceptibility (χ) of radicals **9** and **10** and of σ-dimer **10d** as function of temperature (T) utilizing a Faraday balance; the paramagnetic susceptibility (χ_p) is shown as a function of temperature (Figure 6a [after

(42) Kahr, B.; Engen, D. V.; Mislow, K. *J. Am. Chem. Soc.* **1986**, *108*, 8305−8307.
(43) McBride, J. M. *Tetrahedron* **1974**, *30*, 2009−2022.
(44) Kaupp, G.; Boy, J. *Angew. Chem., Int. Ed* **1997**, *36*, 48−49.
(45) Del Sesto, R. E.; Miller, J. S.; Lafuente, P.; Novoa, J. J. *Chem. Eur. J.* **2002**, *8*, 4894−4808.
(46) Lu, J.; Rosokha, S. V.; Kochi, J. K. *J. Am. Chem. Soc.* **2003**, *125*, 12161−12171.
(47) Jung, Y.; Head-Gordon, Y. *Phys. Chem. Chem. Phys.* **2004**, *6*, 2008−2011.
(48) Miller, J. S.; Zhang, J. H.; Reiff, W. M.; Dixon, D. A.; Preston, L. D.; Reis, A. H.; Gebert, E.; Extine, M.; Troup, J.; Epstein, A. J.; Ward, M. D. *J. Phys. Chem.* **1987**, *91*, 4344−4360.
(49) Novoa, J. J.; Lafuente, P.; Del Sesto, R. E.; Miller, J. S. *Angew. Chem., Int. Ed.* **2001**, *40*, 2540−2543.
(50) Vazquez, C.; Calabrese, J. C.; Dixon, D. A.; Miller, J. S. *J. Org. Chem.* **1993**, *58*, 65−81.
(51) Reed, C. A.; Bolskar, R. D. *Chem. Rev.* **2000**, *100*, 1075−1120.
(52) Konarev, D. V.; Khasanov, S. S.; Otsuka, A.; Saito, G. *J. Am. Chem. Soc.* **2002**, *124*, 8520−8521.

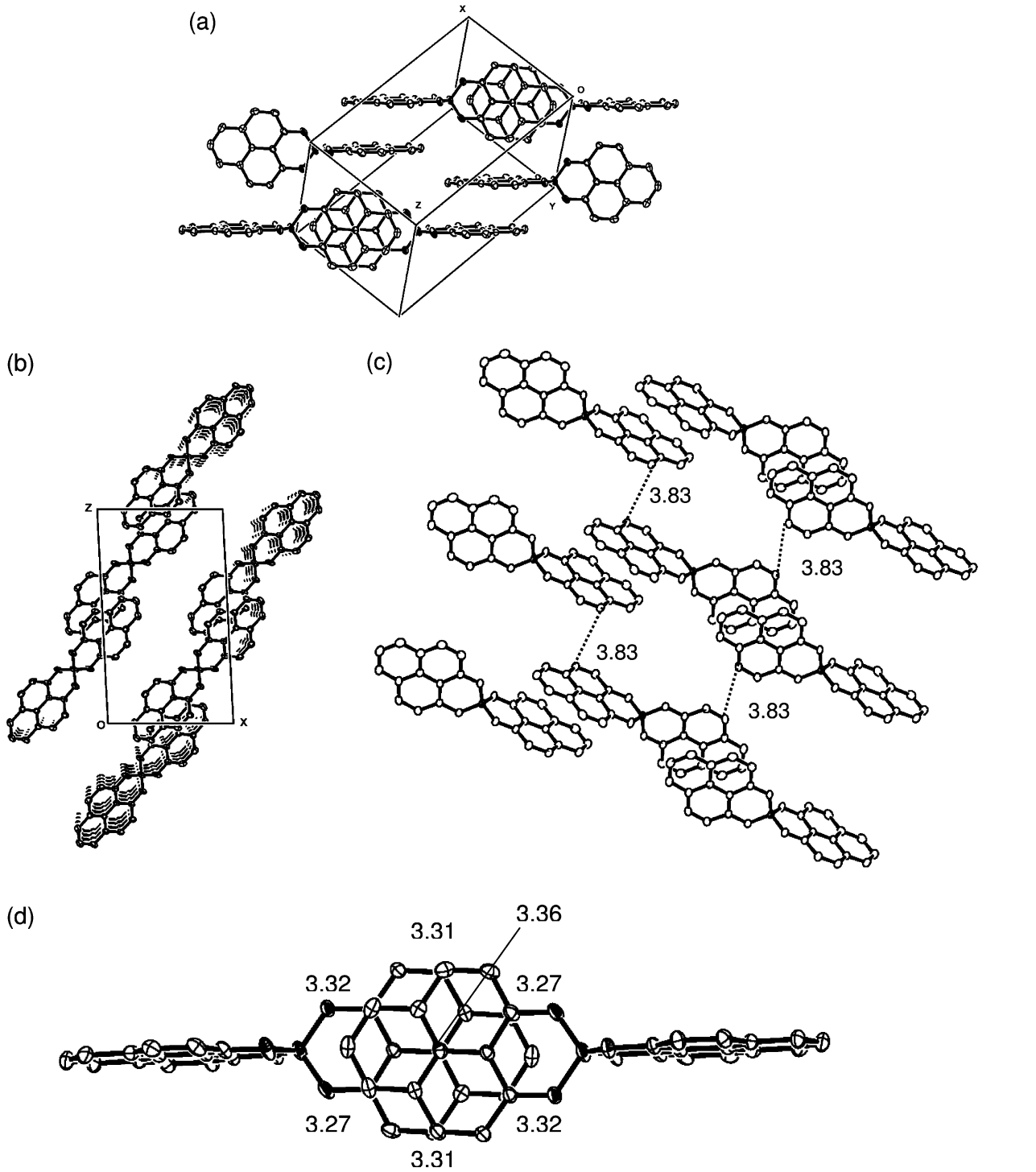

Figure 3. (a) Unit cell of crystalline **9**; viewed normal to the phenalenyl plane. (b) Packing along the *y*-axis. (c) Closest intermolecular C···C contacts (3.83 Å) among the spin-bearing carbon atoms of phenalenyl units between two π-chains of crystalline **9**. (d) Overlap and closest distances of the spin-bearing carbon atoms between pairs of radicals of **9**, with the cycloalkyl groups omitted.

subtraction of the sample diamagnetism]). Pressed pellet conductivity measurements on crystals of **9** and **10** revealed room-temperature conductivities of 1.5×10^{-3} and 1.0×10^{-6} S/cm.

The static paramagnetic susceptibility (χ_p) of crystalline **9** shows practically temperature-independent behavior in the range from 50 to 333 K, and the value of $\chi_p = 450 \times 10^{-6}$ emu/mol is consistent with Pauli paramagnetism; its magnitude is typical of the values obtained for other molecular metals and superconductors and suggests metallic character.[31,53,54] Nevertheless the weak temperature dependence of χ_p with a broad maximum at ~280 K can be fit by the antiferromagnetic 1-D Heisenberg chain model of isotropically interacting spins as we demonstrated in the case of **14** and **15**,[32] and we discuss in detail the

(53) Haddon, R. C.; Ramirez, A. P.; Glarum, S. H. *Adv. Mater.* **1994**, *6*, 316−322.
(54) Murata, T.; Morita, Y.; Fukui, K.; Sato, K.; Shiomi, D.; Takui, T.; Maesato, M.; Yamochi, H.; Saito, G.; Nakasuji, K. *Angew. Chem., Int. Ed.* **2004**, *43*, 6343−6346.

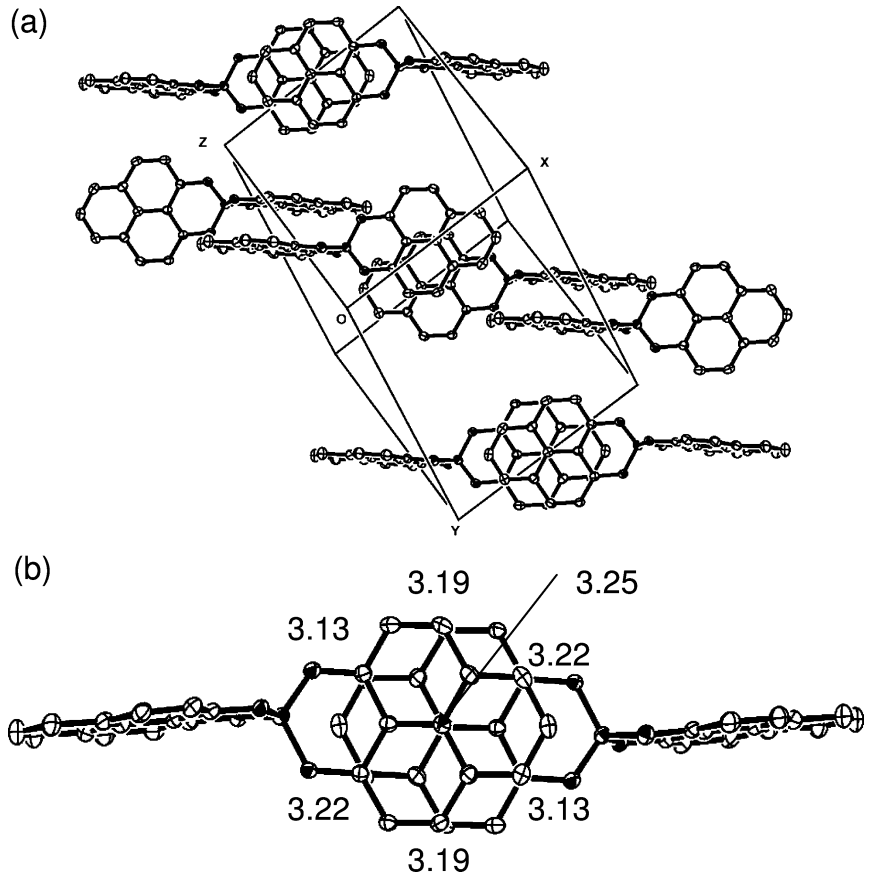

Figure 4. Packing of crystalline **10** showing four pairs of π-dimers: (a) viewed normal to the phenalenyl plane; (b) closest C···C distances (spin-bearing carbon only) within a π-dimer, with cycloalkyl groups omitted.

magnetic properties below. We used the $S = {}^1/_2$ Bonner−Fisher model (BF)[55] in analytical representation[56] to fit $\chi_p(T)$ for compound **9**, with the addition of a term to accommodate the low-temperature Curie tail originating from paramagnetic impurities. On the basis of the fit obtained in the temperature range 50−330 K (Figure 6a), we obtained an intrachain exchange constant $J = -167$ cm^{-1} and a concentration of paramagnetic impurities of 2.4% per molecule in **9**; in the case of **8** we obtained a value of $J = -163$ cm^{-1}.[31] The temperature dependence of the paramagnetic signal corresponds to a linear decrease in the effective number of Curie spins per molecule (obtained from $8\chi_p(T/3)$; Figure 6b).

The paramagnetic signals of π-dimer **10** and the σ-dimer **10d** are much weaker than that of **9** in the temperature range 330−100 K (Figure 6a), and at low temperatures a Curie-type paramagnetic contribution from impurities and structural defects becomes visible. At higher temperatures both compounds behave diamagnetically, and we refer to these structures as the diamagnetic π-dimer (**10**) and the diamagnetic σ-dimer (**10d**). Unlike the ethyl radical (**1**), the cyclooctyl radical **10** does not dissociate to a free radical state in which the coupled spins unpair, and the Curie spin count for **10** remains below 10% up to 400 K.

Optical Measurements of 9, 10, and 10d. To obtain further information on the electronic structure, we measured the absorption spectra of crystalline **9**, **10**, and **10d**. This is possible because of the needlelike morphology of the crystals, some of which are quite thin and are therefore suitable for transmission spectroscopy.

The results are presented in Figure 7, where we show transmittance (T) measurements made on single crystals. The most important feature in the transmission spectra is the strong increase of absorption that occurs between 0.24 eV ($E_{g'}$) and 0.33 eV (E_g) for radical **9**, 0.39 eV ($E_{g'}$) and 0.52 eV (E_g) for radical **10** beyond which the spectrum remains opaque past 10000 cm^{-1} due to very strong bandlike excitations that extend throughout this region of the spectrum (where E_g is the frequency of the absorption onset and $E_{g'}$ is the frequency where the absorption reaches a plateau).

Single-crystal transmittance spectroscopy (Figure 7) shows that the cyclooctyl radical **10** is near-IR opaque, whereas the cyclooctyl σ-dimer **10d** is partially near-IR transparent in the range 3500−10000 cm^{-1}; this technique provided the most straightforward distinction between the crystalline forms. The absorptions in the mid-IR region between 450−3100 cm^{-1} are due to the molecular vibrations; there is a characteristic peak at a frequency of 1635 cm^{-1} in **10d** due to the C═C stretch, which is absent in **10** (Figure 8).

Band Electronic Structure of 9. We carried out extended Hückel theory (EHT) band structure calculation[57] on the crystal structure. Such calculations have been very useful in understanding the electronic structure of organic molecular super-

(55) Bonner, J. C.; Fisher, M. E. *Phys. Rev.* **1964**, *135*, A640.
(56) Estes, W. E.; Gavel, D. P.; Hatfield, W. E.; Hodgson, D. J. *Inorg. Chem.* **1978**, *17*, 1415−1421.
(57) Hofmann, R. *Solids and Surfaces*; VCH: New York, 1988.

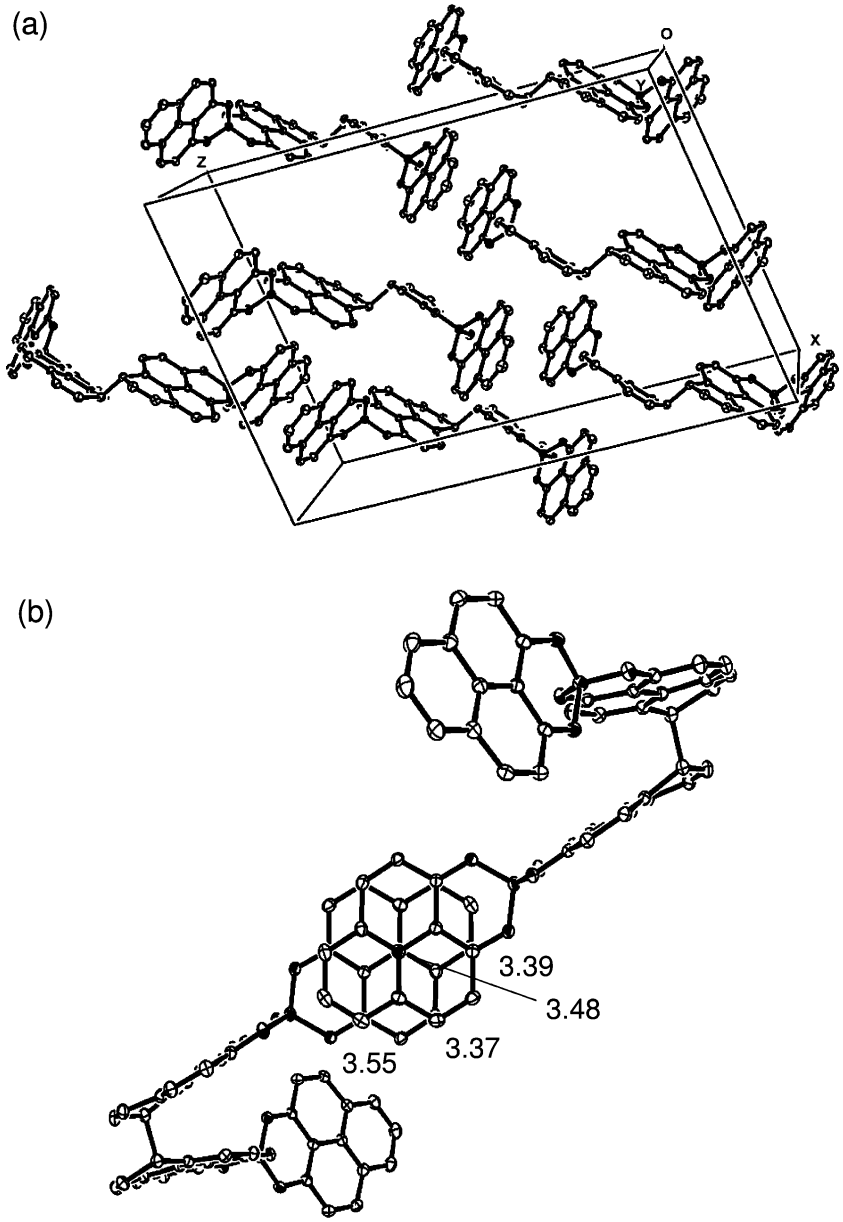

Figure 5. Packing of crystalline **10d**: (a) showing the π-chain interaction between the phenalenyl units; (b) closest intermolecular C···C contacts of phenalenyl units, with the cycloalkyl groups omitted.

conductors[53] and thin-film field effect transistors[58] but cannot be expected to provide a complete picture of the electronic structure in situations where the tight-binding approximation is not applicable.

Figure 9 shows the results obtained from extended Hückel theory (EHT) band structure and DOS calculations carried out on the lattice found in the X-ray crystal structure of **9**. The four bands shown in Figure 9 are derived from the two LUMOs of the cation for each of the two molecules of **9** in the unit cell; basically these consist of the symmetric and antisymmetric combinations of the 1,9-disubstituted phenalenyl LUMO;[24,59] alternatively, they can be viewed as arising from the nonbonding molecular orbitals of each of the four phenalenyl units in the unit cell. In this picture these four orbitals now accommodate a total of two electrons, leading to a quarter-filled band complex, and thus in the discussion below we focus on the lower two levels of Figure 9.

There are substantial band dispersions along the principal directions in reciprocal space in **9** and even greater dispersions along some of the diagonal directions: 0.12 eV [$^1/_2$00], 0.01 eV [0$^1/_2$0], 0.08 eV [00$^1/_2$], 0.22 eV [$^1/_2{}^1/_2{}^1/_2$], whereas the corresponding values in **8** are 0.11 eV [$^1/_2$00], 0.07 eV [0$^1/_2$0], 0.08 eV [00$^1/_2$], 0.28 eV [$^1/_2{}^1/_2{}^1/_2$].[31] While the structural resemblance between **8** and **9** is reflected in their band structures, there is an important difference along b^*: the maximum dispersion in this direction for **8** is 0.07 eV but only 0.01 eV for **9**. This is a reflection of the shortest carbon···carbon distances along the *y*-axis of 3.38 Å for **8** (less than the sum of van der Waals distances for carbon of 3.4 Å) and 3.83 Å for **9**. Thus, there is a clear structural difference between **8** and the newly isolated **9** that is captured by the EHT band structure

(58) Haddon, R. C.; Siegrist, T.; Fleming, R. M.; Bridenbaugh, P. M.; Laudise, R. A. *J. Mater. Chem* **1995**, *5*, 1719−1724.
(59) Haddon, R. C.; Chichester, S. V.; Marshall, J. H. *Tetrahedron* **1986**, *42*, 6293−6300.

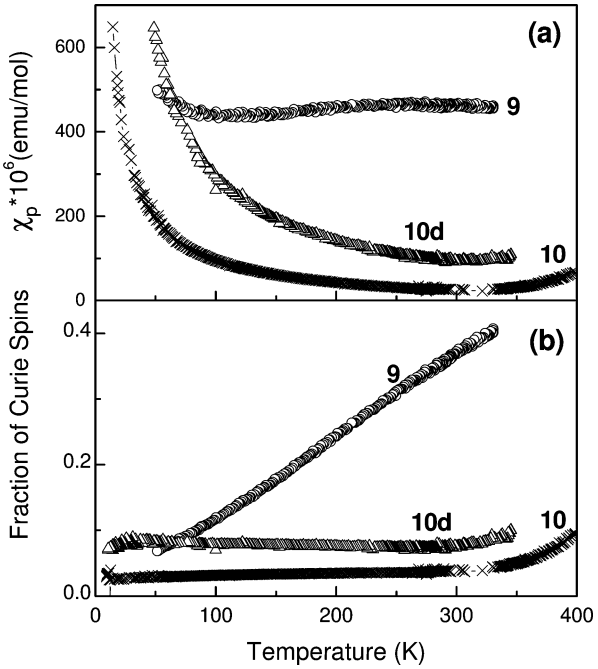

Figure 6. (a) Magnetic susceptibility of **9, 10**, and **10d** as a function of temperature, after correction for diamagnetism. (b) Effective number of Curie spins per molecule [$8\chi_pT/3$], as a function of temperature.

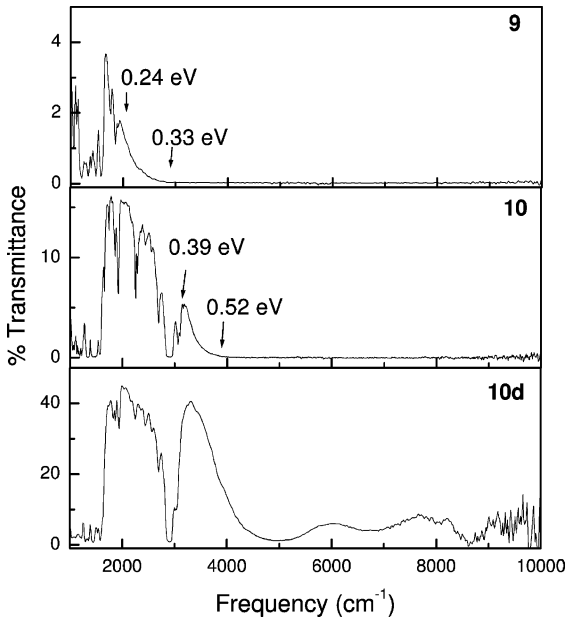

Figure 7. Single-crystal IR and UV−vis transmission spectrum of radical **9**, **10**, and σ-dimer, **10d**.

calculations; however, the common feature for these three compounds is the large bandwidth, $W \approx 0.5$ eV, and the prediction of a metallic ground state that naturally arises from the highly symmetric, periodic structures.

It was noted that the band structures obtained in the DFT calculations on **8** differ in some respects from the previously reported EHT calculations,[31,35,36] and this point is discussed in detail in the Supporting Information. The DFT calculations find a 1-D electronic structure, and this is reflected in the shape of the DOS profile and the small dispersion along [010], in comparison with the bandwidth along the 1-D-π-chain [101].

Our ability to fit the magnetic susceptibility data of **8**, **9**, **14**, and **15** with the Bonner−Fisher linear chain model suggests

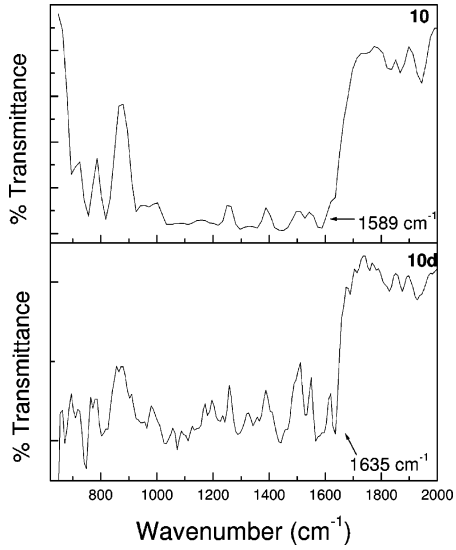

Figure 8. Mid-IR region of single-crystal transmission spectra of cyclooctyl radical **10** and cyclooctyl σ-dimer **10d**.

that there is an underlying relationship between the magnetic properties of the 1-D RVB ground state and the 1-D Heisenberg antiferromagnet—a result that was anticipated by Anderson.[60−62] An essential component of both models is the stability of a highly symmetric ground-state structure which is expected to survive the usual 1-D Peierls distortion.[55,60,62] The delocalized, symmetric nature of the 1-D-π-chain structure of crystalline **8** has recently received theoretical support, and no evidence was found for an incipient Peierls distortion.[36]

According to the Heisenberg Hamiltonian, the interaction energy between two atoms i and j, with spins $\mathbf{S}_i$ and $\mathbf{S}_j$ contains a term

$$V_{ex} = -2J\mathbf{S}_i\cdot\mathbf{S}_j \quad (1)$$

In the 1-D chain problem, the Hamiltonian takes the form

$$H = -2\sum J\mathbf{S}_i\cdot\mathbf{S}_j \quad (2)$$

where the summation is over all nearest neighbors. Basically this is the Hamiltonian used by Pauling in his treatment of resonating valence bonds in organic molecules; it is also the Hamiltonian that is used in the Heisenberg spin-$^1/_2$ antiferromagnet, and because it is equivalent to Heitler−London theory it cannot give electrical conductivity. The present compounds were designed as molecular analogues of the alkali metals.[9,10,63] Anderson concluded that:[61] "In most metals, however, and particularly in the single-electron metals such as the alkalis, the description by the Heitler−London model certainly leads to (2). Then, as we have shown, (2) requires a long-range spin order to be present, which is probably not the case in most metals. Thus, we conclude that the Heitler−London model is not even a good qualitative description of metallic binding, in agreement with Schubin and Wonsowsky[64] and Mott;[65] the band theory must be used in metals, the Heitler−London theory may be used in insulators."

(60) Pauling, L. *Nature* **1948**, *161*, 1019−1020.
(61) Anderson, P. W. *Phys. Rev.* **1952**, *86*, 694−701.
(62) Anderson, P. W. *Mater. Res. Bull.* **1973**, *8*, 153−160.
(63) Haddon, R. C. *Aust. J. Chem* **1975**, *28*, 2333−2342.
(64) Schubin, S.; Wonsowsky, S. *Proc. R. Soc.* (*London*) **1934**, *145*, 159−180.
(65) Mott, N. F. *Proc. Phys. Soc.* (*London*) **1949**, *Ser. A62*, 419−422.

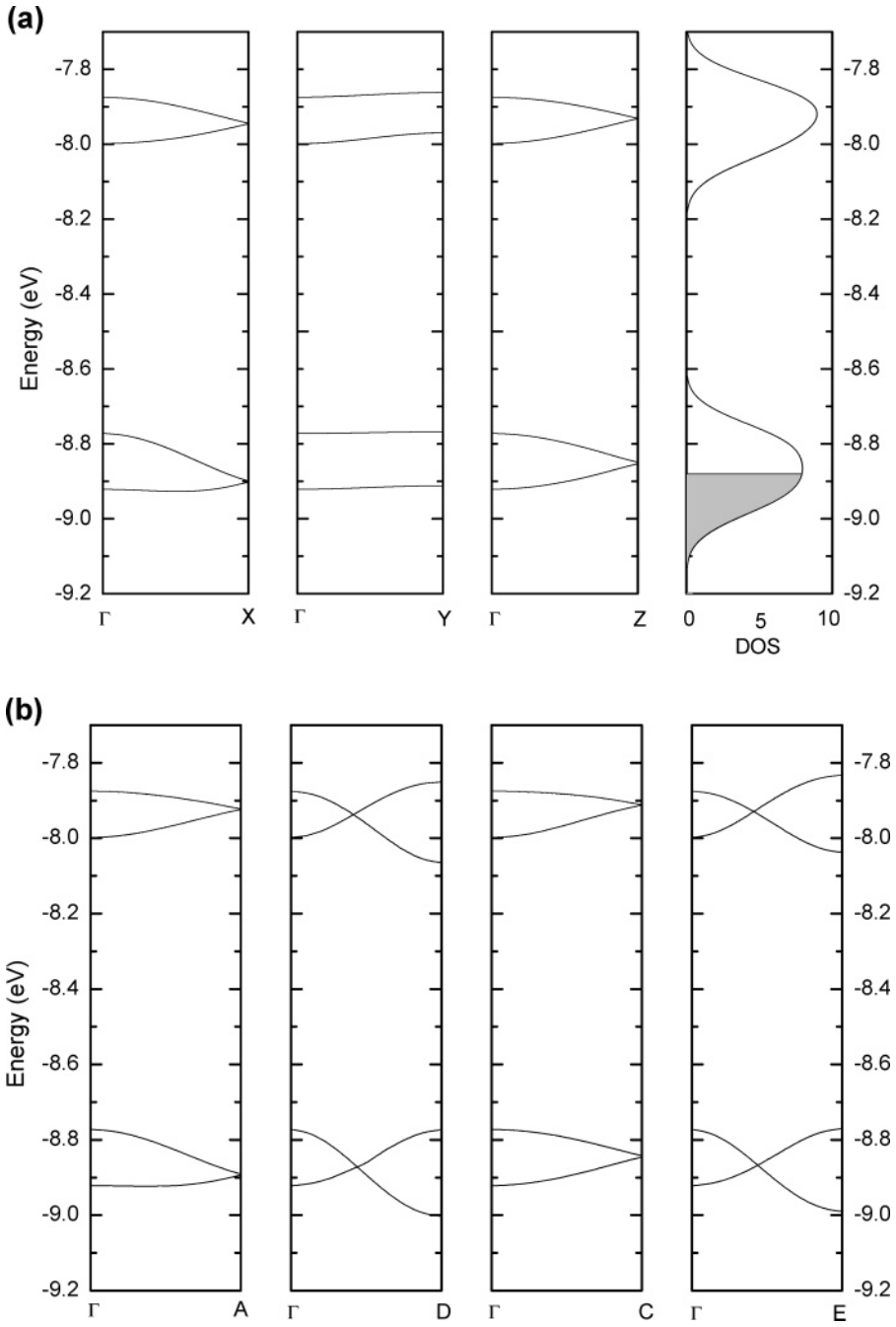

Figure 9. EHT band structure and density of states (DOS) calculated for the experimental structure of crystalline **9**. (a) Dispersions along reciprocal cell axes, where $X = [^1/_2 00]$, $Y = [0^1/_2 0]$, $Z = [00^1/_2]$, and DOS (states/eV mol) (b) Dispersions along diagonal directions, where $A = [^1/_2 {}^1/_2 0]$, $D = [^1/_2 0^1/_2]$, $C = [0^1/_2 {}^1/_2]$, and $E = [^1/_2 {}^1/_2 {}^1/_2]$.

The correct description of materials that fall between the two situations discussed above remains an active area of research under the rubric of strongly correlated electron systems and in principle may be treated by the Hubbard Hamiltonian.[66,67] At large values of U/t the 1-D half-filled-band Hubbard model is related to the Heisenberg linear chain antiferromagnet by the relationship $|J| \approx 2\ t^2/U$,[68,69] where J is the Bonner−Fisher exchange integral, t is the transfer integral ($W \approx 4t \approx 0.4$ eV),[31,35,36] and U is the on-site Coulombic correlation energy, which can be estimated from the electrochemical data to be of order $U \approx 0.4$ eV. Thus, we obtain $2t^2/U \approx 0.05$ eV $= 400$ cm^{-1}, which may be compared with the values of $J \approx -100$ cm^{-1} obtained from the Bonner−Fisher fit to the experimental data for **8**, **9**, **14**, and **15**.[28,32]

Conclusion

By changing the phenalenone substituents, a new family of spiro-bis(1,9-disubstituted phenalenyl)boron neutral radical conductors based on the O, N-ligand system has been synthesized and characterized and the solid-state properties investigated. The disproportionation energies, which largely determine the on-site Coulombic correlation energy in the solid state, are very similar to the alkyl substituted spiro-bis(1,9-disubstituted phenalenyl)boron neutral radicals reported previously (**1**−**6**), but

(66) Anderson, P. W. *Science* **1987**, *235*, 1196−1198.
(67) Cho, A. *Science* **2006**, *314*, 1072−1075.
(68) Ovchinnikov, A. A. *Sov. Phys. JETP Lett.* **1970**, *30*, 1160−1163.
(69) Shiba, H.; Pincus, P. A. *Phys Rev. B.* **1972**, *5*, 1966−1980.

these compounds have an entirely different solid-state structure. Radical (**9**) shows the temperature-independent paramagnetism characteristic of a metal but proved to be a semiconductor, and the properties of **8**, **9**, **14**, and **15** were discussed from the standpoint of the RVB ground state. The dimerization observed for **10** prompted us to review the crystallization of the other neutral spiro-biphenalenyl radicals, but as far as we can tell the behavior of **10** is unique; even when we employed the same conditions for crystal growth that led to **10d**, other members of this series did not produce σ-dimers.

Experimental Section

Materials. Boron trichloride (Aldrich), sodium tetraphenylborate (Aldrich), cobaltocene (Strem), and bis(pentamethylcyclopentadienyl)-nickel(II) (Strem) were all commercial products and were used as received except cobaltocene and bis(pentamethylcyclopentadienyl)-nickel(II) were sublimed under vacuum. 9-Hydroxy-1-oxophenalene was synthesized according to literature procedures.[70] Toluene was distilled from sodium benzophenone ketyl immediately before use. Acetonitrile was distilled from P_2O_5 and then redistilled from CaH_2 immediately before use.

9-*N*-Cycloheptyl-1-oxophenalene (L^1). A mixture of 9-hydroxy-1-oxophenalene (1.5 g, 7.65 mmol) and cycloheptylamine (7 mL) was refluxed for 10 h in argon. Excess amine was removed under vacuum, and the crude product was purified by column chromatography on Al_2O_3 with $CHCl_3$ to give a red oil (2.0 g, 90%). ^{1}H NMR ($CDCl_3$): δ 12.47 (br, 1H), 7.95 (d, 1H), 7.81−7.86 (m, 3H), 7.40 (t, 1H), 7.16 (d, 1H), 6.99 (d, 1H), 3.95−4.03 (m, 1H), 1.55−2.15 (m, 12H).

9-*N*-Cyclooctylamino-1-oxophenalene (L^2). A mixture of 9-hydroxy-1-oxophenalene (1.6 gm, 8.16 mmol) and cyclooctylamine (7 mL) was refluxed for 8 h under argon. The excess amine was removed by distillation under reduced pressure to give a yellow oil. The crude product was purified by column chromatography on Al_2O_3 with $CHCl_3$ to give a yellow oil (2.18 g, 88%). ^{1}H NMR ($CDCl_3$): δ 12.50 (br, 1H), 7.96 (d, 1H), 7.82−7.88 (m, 3H), 7.41 (t, 1H), 7.18 (d, 1H), 7.00 (d, 1H), 3.98−4.06 (m, 1H), 2.06−2.11 (m, 4H), 1.82−1.96 (m, 4H), 1.52−1.65 (m, 6H).

Preparation of 9^+Cl^-. 9-*N*-Cycloheptyl-1-oxophenalene (2.0 g, 6.87 mmol) was dissolved in dry toluene (75 mL) under argon, 1 mL of dry triethylamine was added, followed by the addition of BCl_3 (3.44 mL, 3.44 mmol, of a 1 M solution in dichloromethane). An orange precipitate was formed immediately, and the reaction mixture was stirred 7 h at room temperature. The solid was isolated by filtration, washed several times with dry toluene, and dried under vacuum for 3 h to give 1.8 g (83%) of an orange solid; mp 198 °C. MS (MALDI): *m*/*z* 591. IR (ATR, 4000−600 cm^{-1}): 2928 (w), 2604 (w), 2496 (w), 1629 (s), 1583 (s), 1572 (s), 1516 (s), 1478 (m), 1444 (m), 1366 (m), 1291 (s), 1244 (m), 1189 (w), 1042 (m), 1004 (w), 963 (s), 936 (s), 849 (w), 692 (w).

Preparation of 10^+Cl^-. 9-*N*-Cyclooctylamino-1-oxophenalene (2.18 g, 7.16 mmol) in toluene (50 mL) was treated with boron trichloride in dichloromethane (3.6 mL, 3.58 mmol) in the presence of triethylamine (1 mL) under argon in the dark, and the mixture was stirred at room temperature overnight. The yellow solid was isolated by filtration (1.74 g, 74%); mp 180 °C. MS (MALDI): *m*/*z* 619. IR (ATR, 4000−600 cm^{-1}): 2922 (w), 2603 (w), 2500 (w), 1631 (m), 1584 (m), 1441 (m), 1365 (m), 1289 (s), 1039 (m), 965 (s), 924 (s), 819 (w), 746 (w), 673 (m).

Preparation of $9^+BPh_4^-$. A solution of 0.45 g (1.30 mmol) of $NaBPh_4$ in 10 mL of MeOH was added to a solution of 9^+Cl^- (0.79 g, 1.25 mmol) in 25 mL of MeOH. An orange precipitate formed immediately. The mixture was stirred for 15 min, and 0.29 g (25%) of orange solid was separated by filtration and stored in the dark. The crude product was purified by recrystallization from dichloromethane/methanol mixture; mp 244 °C dec. MS (MALDI): *m*/*z* 591. ^{1}H NMR (CD_3CN); δ 8.56 (d, 2H), 8.31−8.41 (m, 6H), 7.84 (t, 2H), 7.55 (d, 2H), 7.47 (d, 2H), 7.24−7.28 (m, 8H), 6.99 (t, 8H), 6.84 (t, 4H), 3.40−3.58 (m, 2H), 0.89−2.53 (m, 24H). Anal. Calcd for $C_{64}H_{60}B_2N_2O_2.0.5CH_2Cl_2$: C, 81.27; H, 6.44; N, 2.94. Found: C, 80.68; H, 6.40; N, 3.10.

Preparation of $10^+BPh_4^-$. A solution of 1.56 g of $NaBPh_4$ in 20 mL of MeOH was added to a solution of 10^+Cl^- (1.00 g, 1.52 mmol) in 30 mL of MeOH. The mixture was stirred for 15 min, and 0.40 g (28%) of yellow solid was separated and stored in the dark. The yellow product was purified by recrystallization from methanol and dichloromethane mixture; mp 210 °C dec. MS (MALDI): *m*/*z* 619. ^{1}H NMR (CD_3CN): δ 8.59 (d, 2H), 8.31−8.39 (m, 6H), 7.84 (t, 2H), 7.56 (d, 2H), 7.41 (d, 2H), 7.22−7.31 (m, 8H), 6.99 (t, 8H), 6.84 (t, 4H), 3.50−3.66 (m, 2H), 0.70−2.50 (m, 28H). Anal. Calcd for $C_{66}H_{64}B_2N_2O_2.0.5CH_2Cl_2$: C, 81.39; H, 6.68; N, 2.85. Found: C, 81.20; H, 6.68; N, 2.99.

Crystallization of 9. An invertable H-cell with a glass D frit was loaded in a drybox. A solution of 20 mg (0.022 mmol) of $9^+BPh_4^-$ in 10 mL of dry acetonitrile was placed in one container, and 5 mg (0.026 mmol) of $CoCp_2$ dissolved in 10 mL of dry acetonitrile was placed in the other container. The containers were attached to the inverted H-cell in the drybox. The H-cell was removed from the drybox, attached to a vacuum line, and the containers were taken through three cycles of freeze, pump, and thaw to degas the solutions. The H-cell was inverted slowly, and the solutions were allowed to diffuse through the glass frit. After sitting in the dark for 6 days the cell yielded 7 mg (54%) of black needles. Anal. Calcd for $C_{40}H_{40}BN_2O_2$: C, 81.21; H, 6.82; N, 4.74. Found: C, 79.76; H, 6.75; N, 5.23.

Crystallization of 10. An invertable H cell with a glass D frit was loaded in a dry box. A solution of 25 mg (0.027 mmol) of $10^+BPh_4^-$ in 10 mL of dry CH_3CN was placed in one container and 6 mg of $CoCp_2$ (0.030 mmol) dissolved in 10 mL of dry CH_3CN in the other container. The containers were attached to the inverted H cell in the drybox. The H cell was removed from the drybox, attached to a vacuum line, and the containers were taken through three cycles of freeze, pump, and thaw to degas the solutions. The H cell was inverted, and the solutions were allowed to diffuse through the glass frit. After sitting in the dark for 1 week the cell yielded 9 mg (54%) of black needles. Anal. Calcd for $C_{42}H_{44}BN_2O_2$ CH_3CN: C, 79.99; H, 7.17; N, 6.36. Found: C, 79.63; H, 7.02; N, 6.72.

Crystallization of 10d. The crystallization procedure for **10d** is the same as that used for **10** except Cp^*_2Ni was used instead of $CoCp_2$ (yield = 71%). Anal. Calcd for $C_{84}H_{88}B_2N_4O_4$: C, 81.41; H, 7.16; N, 4.52. Found: C, 80.97; H, 7.14; N, 4.80.

Cyclic Voltammetry. Cyclic voltammetric measurements were performed with a Pine AFCBP1 potentiostat using a Pt wire electrode in dry acetonitrile under an argon atmosphere with *n*-Bu_4NPF_6 as the supporting electrolyte and employing a standard calomel reference electrode. The ferrocenium/ferrocene couple was used as internal reference, and the scan rate was 100 mV/s.

X-ray Crystallography. Data were collected on a Bruker SMART 1000 platform-CCD X-ray diffractometer system (Mo radiation, λ = 0.71073 Å, 50 kV/40 mA power). The crystals were coated with paratone oil and mounted on glass fibers. The crystallographic parameters and the unit cell dimensions are summarized in Table 1. Absorption corrections were applied to the raw intensity data using the SADABS program in the SAINTPLUS software package.[71] The Bruker SHELXTL (Version 6.10) software package[72] was used for phase determination and structure refinement. Atomic coordinates, isotropic and anisotropic displacement parameters of all the non-hydrogen atoms were refined by means of a full matrix least-square procedure on F^2. All H-atoms were included in the refinement in calculated positions riding on the atoms to which they were attached. Full details, including bond lengths and bond angles, are given in the Supporting Information.

(70) Haddon, R. C.; Chichester, S. V.; Mayo, S. L. *Synthesis* **1985**, 639−641.

(71) 5.02 ed.; Bruker Analytical X-Ray System, Inc: Madison, WI, 1997−1998.
(72) 6.10 ed.; Bruker Analytical X-Ray System, Inc.: Madison, WI, 2000.

Magnetic Susceptibility Measurements. The magnetic susceptibility was measured on a George Associates Faraday balance operating at 0.5 T in the temperature range 5 K−400 K. The system was calibrated using Al and Pt NIST standards. The paramagnetic components of the magnetic susceptibility (χ_p) of **9**, **10**, and **10d** (Figure 6) were obtained after subtraction of the calculated diamagnetic core contribution: -365.6×10^{-6} emu/mol, -385.5×10^{-6} emu/mol and -771×10^{-6} emu/mol for **9, 10**, and **10d**, respectively, utilizing published values for Pascal's constants.[73] The concentration of ferromagnetic impurities was found to be less than 2 ppm for all compounds, by measurement of the intercept of the nonlinear component of the field dependence of χ. While the ferromagnetic term was small, this correction was made to the measured total force. The concentration of paramagnetic impurities was evaluated by analyzing the low-temperature Curie tails, and values of 2.4% and 4% for were found for compounds **9** and **10**, respectively. For the σ-dimer **10d** the low-temperature paramagnetic tail is more pronounced, and the high concentration of the paramagnetic defects (10%) corresponds to the incomplete σ-bonding of ~5% of the dimers. The increase of χ in **10** and **10d** (Figure 6) at high temperatures corresponds to the beginning of the sample decomposition.

Single-Crystal IR and UV−Vis Transmission Spectroscopy. The infrared transmission measurements were carried out on an FTIR Nicolet Nexus 670 ESP spectrometer integrated with a Continuum Thermo-Nicolet FTIR microscope.

Band Structure Calculations. The band structure calculations made use of a modified version of the extended Hückel theory (EHT) band structure program supplied by M. H. Whangbo and are discussed in more detail in the Supporting Information. The parameter set is chosen to provide a reasonably consistent picture of bonding in heterocyclic organic compounds.[58,74] The EHT calculations used a Gaussian smoothing factor to obtain the DOS curve from k-point grids that were chosen on the basis of the Patterson space group.[75]

Acknowledgment. This work was supported by the Office of Basic Energy Sciences, Department of Energy, under Grant DE-FG032-97ER45668 and by DOD/DARPA/DMEA under Award No. DMEA 90-02-2-0216.

Supporting Information Available: Tables of crystallographic and structure refinement data, atomic coordinates, bond lengths and angles, anisotropic thermal parameters, band structure analysis, and full literature citatation (for ref 3); complete set of fitting parameters to the magnetic susceptibility data of **9**; CIF files of structures **9**, **10**, and **10d**. This material is available free of charge via the Internet at http://pubs.acs.org.

JA070103I

(73) Carlin, R. L. *Magneto-Chemistry*; Springler-Verlag: Berlin-Heidelberg-New York-Tokyo, 1986.

(74) Cordes, A. W.; Haddon, R. C.; Oakley, R. T.; Schneemeyer, L. F.; Waszczak, J. V.; Young, K. M.; Zimmerman, N. M. *J. Am. Chem. Soc.* **1991**, *113*, 582−588.

(75) Ramirez, R.; Bohm, M. C. *Int. J. Quant. Chem.* **1988**, *34*, 571−594.